Atmos. Chem. Phys. Discuss., 9, 25127–25158, 2009
www.atmos-chem-phys-discuss.net/9/25127/2009/

Atmospheric Chemistry and Physics Discussions

This discussion paper is/has been under review for the journal Atmospheric Chemistry and Physics (ACP). Please refer to the corresponding final paper in ACP if available.

Heavy ozone enrichments from MIPAS limb emission spectra

C. Piccolo[1,*], **A. Dudhia**[1], **and V. H. Payne**[2]

[1]Atmospheric, Oceanic and Planetary Physics, University of Oxford, Oxford, UK
[2]Atmospheric and Environmental Research Inc., Lexington, MA, USA
[*]now at: Met Office, Exeter, UK

Received: 30 September 2009 – Accepted: 10 November 2009 – Published: 25 November 2009

Correspondence to: C. Piccolo (piccolo@atm.ox.ac.uk)

Published by Copernicus Publications on behalf of the European Geosciences Union.

Abstract

Vertical enrichment profiles of stratospheric heavy ozone (asymmetric and symmetric $^{50}O_3$ isotopomers) have been derived from the Michelson Interferometer for Passive Atmospheric Sounding (MIPAS). As a continuously operating satellite instrument, MIPAS has an advantage over previous measurements in providing global coverage over an extended time period, allowing the variations in enrichment to be determined. However, since the spectral features of the isotopomers are comparable with the magnitude of the instrument noise, a sequential estimation retrieval scheme has been used to average the measurements zonally.

The magnitude of observed enrichments is ∼10% in stratosphere, a value consistent with previous observations and lab measurements. The data indicate that asymmetric heavy ozone is significantly more enriched than the symmetric isotopomer and show latitudinal and vertical variations in both the asymmetric and symmetric $^{50}O_3$ enrichments. Enrichments decrease with decreasing temperature, as previously noted, at midlatidudes and polar regions, while they increase with decreasing temperature in equatorial regions.

MIPAS measurements contain also information on the asymmetric and symmetric $^{49}O_3$ isotopomers. The enrichments of $^{49}O_3$, obtained with the same sequential estimator approach, are much larger than the enrichments of $^{50}O_3$, in contraddictions with previous results which predict larger enrichments for heavier isotopomers.

1 Introduction

1.1 Ozone isotopologues

Atmospheric "heavy" ozone is enriched in the isotopes ^{18}O and ^{17}O. These enrichments were first observed more than 20 years ago in the two atmospherically significant isotopologues $^{49}O_3$ and $^{50}O_3$, in which one ^{16}O atom is replaced by either an ^{17}O or an

ACPD

9, 25127–25158, 2009

^{18}O atom respectively (Mauersberger, 1981; Thiemens and Heidenreich, 1983). The enhancements (~10%) of heavy ozone are the most prominent feature in the isotopic chemistry in the stratosphere. This large oxygen isotopic signature can be transfered from ozone to other trace gases, such as CO_2, CO and N_2O (Yung et al., 1991, 1997). Therefore their isotopic composition can serve as markers for atmospheric transport and chemical reactions.

Starting with the isotopic ratio R, i.e. the ratio of the concentration of the minor to the major isotopologue (e.g. $[^{50}O_3]/[^{48}O_3]$), the ozone enrichment, δ, is usually defined as:

$$\delta(\%) = 100 \cdot \left(\frac{R}{R_0} - 1 \right) \quad (1)$$

where R_0 is some reference value of the isotopic ratio. While the choice of reference standard is arbitrary, clearly the same standard has to be used when comparing different measurements. In line with previous studies in the present work we choose the oxygen isotopic composition in atmospheric O_2 as our standard, rather than SMOW (Standard Mean Ocean Water) which is used, for example, in the HITRAN spectroscopic database.

The relative abundances of oxygen atoms ^{16}O:^{18}O:^{17}O are approximately 1:1/500:1/2700 in both standards (although atmospheric O_2 is enriched in ^{18}O by 2.35% and in ^{17}O by 1.175% compared to SMOW). Therefore, the reference ratio R_0 for molecular oxygen containing an atom of the ^{18}O isotope is approximately 2/500, and 3/500 for ozone.

However, unlike molecular oxygen, there are two distinct arrangements ("isotopomers") for a singly substituted ozone. Using Q to denote the heavy oxygen atom, these are the symmetric (OQO) or asymmetric (QOO) isotopomers, depending on whether the middle or an end atom is substituted. Since there is twice the likelihood of a randomly substituted atom being at the end rather than the middle, the reference ratios for these two isotopomers are split accordingly (e.g. if Q is ^{18}O, 1/500 for OQO

and 2/500 for QOO, totalling 3/500 as before).

Conversely, given measured enhancements δ(OQO) and δ(QOO) in the two isotopomers, the total isotopic enhancement δQ is calculated as

$$\delta Q = \frac{1}{3}\delta(OQO) + \frac{2}{3}\delta(QOO) \quad (2)$$

It is now well established both in the atmosphere and in the laboratory that when ozone is formed from O and O_2 via the three-body (Chapman) reaction, there is a preference for the formation of heavy ozone (Mauersberger et al., 2001; Lämmerzahl et al., 2002; Janssen et al., 2003).

1.2 Fractionation processes

In stratosphere, the ozone chemistry is governed by the reaction cycle:

$$O + O_2 + M \rightarrow O_3 + M \quad (R1)$$

where M is a third body. The corresponding reactions for heavy ozone are:

$$Q + O_2 + M \rightarrow OOQ + M \quad (R2)$$
$$O + OQ + M \rightarrow OQO + M \quad (R3)$$
$$\rightarrow OOQ + M \quad (R4)$$

As noted by Kaye and Strobel (1983), we must also consider the exchange reactions:

$$Q + O_2 \rightleftharpoons O + OQ \quad (R5)$$

Whenever oxygen atoms are available to form ozone, fast isotope exchange reactions (Reaction R5) will rapidly recycle the atoms through many molecules before ozone is produced by collisional stabilization of an atom-diatom pair. At 100 hPa pressure, the exchange reactions are about 2000 times faster than ozone formation. Janssen et al. (2001) stated that the large variability of the formation rate coefficients

relative to the standard ozone formation process (Reaction R1) of about 50% characterises the ozone isotope effect and demonstrates its kinetic origin.

Photo-chemical modeling has shown that photolysis also contributes to fractionation at low pressure (e.g. stratosphere), and that photolysis-induced fractionation can result in high enrichment although an order of magnitude less than enrichments resulting from formation (Bhattacharya et al., 2002; Liang et al., 2006).

A number of isotope fractionation processes have a predicatable mass-dependence. Because the vibrational frequencies of a chemical bond depend on the masses of the atoms that form that bond, the heavy isotopes are usually more tightly bound, which leads to fractionation in chemical reactions. In the case of oxygen with its three stable isotopes (^{16}O, ^{17}O, ^{18}O), such mass-dependent effects cause relative differences in enhancements (using the notation of Eq. 1) $\delta^{17}\mathrm{O} \sim 0.52\delta^{18}\mathrm{O}$ (Kaye and Strobel, 1983) which, for example, explains the relative differences between the SMOW and molecular oxygen standard reference ratios. However, Thiemens and Heidenreich (1983) discovered that the formation of ozone deviates from the expected mass dependent fractionation. The surprising fact that the ^{18}O and ^{17}O are enriched in the ozone approximately equally ($\delta^{18}\mathrm{O} \sim \delta^{17}\mathrm{O}$), rather than in a 2:1 ratio, led to the concept of mass independent fractionation in chemical reactions. Since then numerous investigations established that both tropospheric and stratospheric ozone exhibit mass independent fractionation (Johnston and Thiemens, 1997; Mauersberger et al., 2001).

1.3 Previous measurements

Stratospheric enrichment of heavy ozone was first reported by Mauersberger (1981) using a balloon-borne mass spectrometer. Further stratospheric enrichments were reported based on mass spectrometry (Krankowsky et al., 2000; Mauersberger et al., 2001; Lämmerzahl et al., 2002), far-infrared emission spectroscopy (Abbas et al., 1987; Carli and Park, 1988; Johnson et al., 2000), cryogenic grab-sampling (Schueler et al., 1990), ground-based (Meier and Notholt, 1996) and space-based solar spectroscopy (Irion et al., 1996). Both far-infrared (Johnson et al., 2000) and ATMOS (Irion

et al., 1996) measurements show no statistically significant variation with latitude, altitude and time, while they indicate that asymmetric heavy ozone is significantly more enriched than the symmetric isotopomer. Newly available high resolution measurements of ozone isotopic composition made at mid-latitudes (Krankowsky et al., 2000; Mauersberger et al., 2001; Lämmerzahl et al., 2002) show instead that the magnitude of the enrichments increases with altitude. Mauersberger et al. (2001) attempted to explain the altitude variation of the enrichments by temperature variations.

Heavy ozone enrichment has also been observed in laboratory measurements (Mauersberger et al., 1999; Thiemens and Heidenreich, 1983; Morton et al., 1990; Anderson et al., 1997; Janssen et al., 2003). The temperature and pressure dependence of the formation rate coefficients of Reactions (R2) and (R3) relative to the formation of standard ozone (R1) have been explored in laboratory by Morton et al. (1990). They have shown that enrichment decreases with decreasing temperature and increasing pressure. In the stratosphere, since the pressure of interest is less than 50 mbar (altitudes greater than 20 km), the formation rates of ozone are close to their low-pressure limit, the pressure dependence is insignificant.

1.4 This study

This paper presents an analysis of spectra from a new satellite instrument, MIPAS, to determine the concentrations of the symmetric and asymmetric isotopomers of $^{50}O_3$. Although the signal/noise in individual spectra is low compared to previous instruments, the continuous global dataset of MIPAS allows the full meridional and seasonal variations in isotopic concentration to be observed for the first time with a single instrument.

Section 2 describes the MIPAS instrument and retrieval methodology and Sect. 3 the error analysis. In Sect. 4 the results are compared with previous measurements and in Sect. 5 the full dataset is analysed for possible correlations with other atmospheric parameters. Some results for the $^{49}O_3$ isotopomers are briefly discussed in Sect. 6. Section 7 contains the conclusions.

ACPD
9, 25127–25158, 2009

2 Retrieval of heavy ozone

2.1 The MIPAS instrument

The Michelson Interferometer for Passive Atmospheric Sounding (MIPAS) (ESA, 2000) is a fourier transform spectrometer on the Envisat satellite. Envisat was launched in March 2002 and is in a sun-synchronous polar orbit, crossing the equator in the southward direction at mean local solar time 10:00 a.m. MIPAS acquires spectra over the range 685–2410 cm^{-1} (14.6–4.1 μm), which includes the vibration-rotation bands of many molecules of interest. It is capable of measuring continuously around an orbit in both day and night and includes some azimuth scanning to extend coverage to the poles. Each orbit takes approximately 100 min, giving approximately 14 orbits in 24 h during which almost complete global coverage is obtained.

Although primarily intended as an instrument for monitoring the concentrations of the major stratospheric gases, these spectra also contain information on their isotopologues and many other molecules of interest. MIPAS measurements have been already used to retrieve the deuterium content in water vapor (HDO or δD) in the stratosphere and upper troposphere (Steinwagner et al., 2007; Payne et al., 2007).

From July 2002 until March 2004 MIPAS was operated at "full" spectral resolution (sampling spectra at 0.025 cm^{-1}) with a nominal limb-scanning sequence of 17 spectra taken at tangent heights from 68 km down to 6 km with 3 km spacing in the troposphere and stratosphere. In March 2004 operations were suspended following problems with the interferometer slide mechanism and, although later resumed at reduced spectral resolution, only the full-resolution spectra are analysed here.

2.2 Optimal estimation

The retrieval code used in this study is the MIPAS Orbital Retrieval using Sequential Estimation (MORSE). This is similar to that used for the ESA operational processing scheme (Ridolfi et al., 2000) in that it also uses microwindows (Dudhia et al., 2002b)

ACPD
9, 25127–25158, 2009

and pretabulated absorption coefficients (Dudhia et al., 2002a) derived from the same spectroscopic database (Flaud et al., 2003), but the essential difference is that it is an optimal estimation scheme (Rodgers, 2000) rather than an unconstrained least-squares fit.

In simplified linear form, an optimal estimation solution represents the minimisation of a cost function χ^2 given by:

$$\chi^2 = (\boldsymbol{y} - \mathbf{K}\boldsymbol{x})^T \mathbf{S}_y^{-1} (\boldsymbol{y} - \mathbf{K}\boldsymbol{x}) + (\boldsymbol{x} - \boldsymbol{x}_a)^T \mathbf{S}_a^{-1} (\boldsymbol{x} - \boldsymbol{x}_a) \quad (3)$$

where $\boldsymbol{y}$ is the vector of measurements (i.e. radiance spectra), $\boldsymbol{x}$ the atmospheric state vector (i.e. concentration profile) to be retrieved, $\boldsymbol{x}_a$ is some a priori estimate of $\boldsymbol{x}$, $\mathbf{K}$ is the *Jacobian* matrix (derivatives $\partial \boldsymbol{y} / \partial \boldsymbol{x}$), $\mathbf{S}_y$ is the error covariance of the measurements (i.e. instrument noise) and $\mathbf{S}_a$ the error covariance of the a priori estimate $\boldsymbol{x}_a$. The first term is the cost of the solution $\boldsymbol{x}$ deviating from the measurements and the second term the cost of deviating from the a priori estimate. This has a solution and associated covariance $\mathbf{S}_x$ given by

$$\boldsymbol{x} = \boldsymbol{x}_a + \left(\mathbf{K}^T \mathbf{S}_y^{-1} \mathbf{K} + \mathbf{S}_a^{-1} \right)^{-1} \mathbf{K}^T \mathbf{S}_y^{-1} (\boldsymbol{y} - \mathbf{K}\boldsymbol{x}_a) \quad (4)$$

$$\mathbf{S}_x = \left(\mathbf{K}^T \mathbf{S}_y^{-1} \mathbf{K} + \mathbf{S}_a^{-1} \right)^{-1} \quad (5)$$

The MORSE retrieval actually uses a non-linear iterative scheme but the same principles apply.

For strong signals, such as from the main infrared bands of $^{48}O_3$, the inclusion of the a priori estimate and associated covariance (typically representing ±100% uncertainty) acts simply as a numerical constraint and the actual solution is, for practical purposes, the same as obtained from a least squares fit (the limit of $\mathbf{S}_a^{-1} \rightarrow 0$ in the above equations).

ACPD
9, 25127–25158, 2009

2.3 Sequential estimation

When attempting retrievals from weak spectral features (small **K** values), the advantage of the optimal estimation technique is that it adds stability to the inversion, but at the expense of introducing a bias from the a priori estimate, often taken from climatology. This prevents any simple averaging of retrieved profiles in order to reduce the signal/noise.

Conceptually, the simplest solution would be to average the radiances before the retrieval but, in practice, the actual radiances are highly non-linear functions of the atmospheric state (temperature, tangent point pressure etc.) so such a retrieval is unlikely to match the true mean state of the atmosphere.

The optimal estimation technique provides a suitable framework for a third method which avoids both these problems by starting with climatological a priori estimate and then continues the averaging process in state space (i.e. profile by profile) as more measurements are added. This is the principle of sequential estimation (Rodgers, 2000).

The sequential estimator uses the optimal estimation equations (Eqs. 4, 5) except that the a priori estimate is replaced by the output of the previous retrieval. After $i-1$ profiles have been averaged, the measurements $\boldsymbol{y}_i$ for the ith profile are incorporated into an updated estimate $\boldsymbol{x}_i$ as follows:

$$\boldsymbol{x}_i = \boldsymbol{x}_{i-1} + \left(\mathbf{K}_i^T \mathbf{S}_{yi}^{-1} \mathbf{K}_i + \mathbf{S}_{i-1}^{-1}\right)^{-1} \mathbf{K}_i^T \mathbf{S}_{yi}^{-1} \left(\boldsymbol{y}_i - \mathbf{K}_i \boldsymbol{x}_{i-1}\right) \quad (6)$$

and similarly for the covariance.

The sequential estimator is a particular case of the Kalman filter, where the matrix describing the evolution operator that transform $\boldsymbol{x}_{i-1}$ into $\boldsymbol{x}_i$ is simply persistence, i.e. the identity matrix.

2.4 Implementation

The first step is to run the normal optimal estimation retrieval to generate a set of "standard" profiles of pressure, temperature, H_2O, O_3, CH_4 and N_2O, using the same microwindows as the ESA processor (these microwindows do not distinguish between isotopologues but the resulting O_3 profiles are assumed to be predominantly $^{48}O_3$).

The "standard" ozone profiles are then used to provide an improved "climatological" a priori to initiate the sequential estimator. The same a priori profile is used for all isotopomers (i.e. the a priori enrichments are assumed to be zero) but the a priori uncertainty is set to ±10% for $^{48}O_3$ and ±100% for the other isotopic variants.

The various isotopomers of ozone, including $^{48}O_3$, are then retrieved simultaneously using the sequential estimator and a different, dedicated set of microwindows (Table 1). For each retrieval, the forward model uses the corresponding standard profiles for pressure, temperature, H_2O, CH_4 and N_2O, and climatological values for other interfering species. The sequential estimator is run for all spectra within 10 degree latitude bins in a single day, effectively averaging about 50 individual profiles hence resulting in approximately a factor 7 reduction in S/N compared to a single profile retrieval.

3 Error analysis

3.1 Microwindow selection

Microwindows are the small subsets (typically a few cm^{-1} width) of the complete MIPAS spectrum which are used for the retrievals of particular species. Ideally, these microwindows represent regions of the spectrum with maximum information content on the target molecule and minimum contribution from systematic errors, such as interfering lines of other molecules.

The selection algorithm developed for MIPAS (Dudhia et al., 2002b) is based on modeling the propagation of a large number of potential sources of systematic errors

ACPD
9, 25127–25158, 2009

as well as random noise, through the retrieval process.

Here, the selection was based on a joint retrieval of the main isotopomer ($^{48}O_3$) with the other singly substituted isotopic variants. Normally the selection scheme generates microwindows for a single profile retrieval so, to simulate the sequential estimator retrieval the assumed instrument noise was reduced by a factor 7.

A byproduct of the selection scheme is a detailed error analysis showing the contribution of all considered sources of error to the final product:

$$\mathbf{S}_x^{\text{tot}} = \mathbf{S}_x^{\text{rnd}} + \sum_j \mathbf{S}^{\text{sys}(j)} \tag{7}$$

where the total error covariance is expressed as the sum of the random error plus various independent systematic error terms. The square roots of the diagonals of these matrices represent the error profiles which are shown in Fig. 1, from which we conclude that the retrieval accuracy is limited by the systematic rather than random errors for all three isotopomers and, in the mid-stratosphere, specifically the error arising from the assumption that the atmosphere is horizontally homogeneous during the retrieval (the "GRA" error, shown in the figures, is that which arises from the difference in radiance if a "typical" 1 K/100 km horizontal temperature gradient is imposed on the atmosphere).

3.2 Error analysis on δ values

The enrichment profile δ is, apart from scaling factors and constants, the ratio of two retrieved profile x/z where x is the concentration of the minor isotopomer and z the concentration of $^{48}O_3$. In linearised form, the corresponding error covariance in enrichment, $\mathbf{S}_\delta$ is therefore given by

$$\mathbf{S}_\delta = \mathbf{J}^T \mathbf{S} \mathbf{J} = \left(\frac{\partial\delta}{\partial x}, \frac{\partial\delta}{\partial z} \right) \begin{pmatrix} \mathbf{S}_{xx} & \mathbf{S}_{xz} \\ \mathbf{S}_{xz} & \mathbf{S}_{zz} \end{pmatrix} \begin{pmatrix} \frac{\partial\delta}{\partial x} \\ \frac{\partial\delta}{\partial z} \end{pmatrix} \tag{8}$$

where covariance matrices $\mathbf{S}_{xx}$ and $\mathbf{S}_{zz}$ represent the error correlations *within* the profiles of x and z respectively, and $\mathbf{S}_{xz}$ represents the error correlations between the two,

all of which are submatrices of the error covariances generated by the microwindow selection (Eq. 7).

J is a matrix containing the derivatives of each element δ with respect to each element of x and z although for any profile level i the only non-zero elements will be those relating to the equivalent altitudes in x and z. Taking the asymmetric isotopomer as an example, using R=[QOO]/[O_3] and Eq. (1), these terms are

$$\frac{\partial\delta(\mathrm{QOO})_i}{\partial[\mathrm{QOO}]_i} = \frac{1}{[\mathrm{O_3}]_i} \cdot \frac{100}{R_0} \tag{9}$$

$$\frac{\partial\delta(\mathrm{QOO})_i}{\partial[\mathrm{O_3}]_i} = \frac{-[\mathrm{QOO}]_i}{[\mathrm{O_3}]_i^2} \cdot \frac{100}{R_0} \tag{10}$$

Similar considerations have been applied to error analyses of the retrieval of the deuterium enrichment of water vapour from MIPAS (Payne et al., 2007; Steinwagner et al., 2007).

The above analysis has been applied to each of the error covariances from the microwindow selection to give the equivalent set of error profiles for the enrichment values, and the results are shown in Fig. 2.

Comparing these plots with the individual error analyses in Fig. 1 it can be seen that, as expected, the random error in the ratio is limited by the random error in the minor isotopomer (compared to which the random error contributed by $^{48}O_3$ would be negligible). However, many types of systematic error have been reduced by taking the ratio. For example, the error due to neglecting horizontal temperature gradients tend to affect both major and minor isotopomers by proportionally the same amount, and so largely cancels out in the ratio. However, the errors due to instrument calibration effects, which are assumed uncorrelated between microwindows, benefit less from the cancellation and so start to become more significant in the ratio.

It should be emphasised that several of these systematic error sources are not well-characterised, particularly the estimates of the uncertainties in spectroscopic parameters (SPECDB) and the instrument lineshape (SPREAD), although the latter is likely

ACPD
9, 25127–25158, 2009

to be an overestimate. Other errors may be well-represented as systematic errors for single profiles but become pseudo-random errors when several profiles are averaged: the errors due to the propagation of retrieved temperature (TEM) and pressure (PRE) uncertainties are examples of this. Their treatment as a constant systematic error is likely to be an overestimate and it could be argued that their amplitude should be reduced by the same $\sqrt{50}$ factor. The error due to horizontal inhomogeneity (GRA) is only based on a typical temperature gradient and, considering that each latitude band consists of an equal number of ascending and descending orbits, the actual impact on the zonal average would be much reduced compared to a single profile.

However, there are other errors which are not included in this analysis. Most significant of these is likely to be the "smoothing" error, caused by the inability of the retrieval to fully reproduce the true vertical structure, which would be more significant when forming a ratio of two profiles with different averaging kernels. Secondly the assumption of a zonally symmetric atmospheres may fail when perform the sequential estimation: for example, given that the S/N is lower for colder atmospheres (smaller radiances for a given concentration), a sequential estimator would be biased towards the isotopomer concentrations of the warmer sectors.

So, although the plots suggest that the zonal mean enrichments can be retrieved to accuracies of the order of 1% between 20–50 km, the error analysis cannot be regarded as definitive.

4 Comparison with previous measurements

4.1 FIRS-2

FIRS-2 (Johnson et al., 1995) is a far-infrared Fourier transform spectrometer which has been used to measure atmospheric emission spectra from both aircraft and balloon platforms. The spectrometer resolution of 0.004 cm^{-1} (unapodized) is sufficient to resolve individual rotational transitions of ozone lines. Over the altitude range 25–35 km

the average enhancements for for asymmetric, symmetric and total $^{50}O_3$ were found to be 12.2±1.0%, 6.1±1.8% and 10.2±0.9%, respectively (Johnson et al., 2000). FIRS-2 measurements of $^{50}O_3$ show no significant variation with altitude or time.

Figure 3 shows a comparison of MIPAS results with the averaged enrichments from six balloon flights which took place between 1989 and 1994, at latitudes from 30–35° N. Here the MIPAS data have been averaged for the same months and latitudes as the FIRS-2 measurements. The enrichments are in agreement in stratosphere (over the range of about 25–40 km), while MIPAS shows lower enrichments below 25 km.

4.2 MIPAS-Balloon

MIPAS-B (Friedl-Vallon et al., 2004), the balloon-borne version of the MIPAS satellite instrument, was flown from Aire sur l'Adour, France (43.7° N) on 24 September 2002, and from Kiruna, Sweden (67.5° N) on 20/21 March 2003 as part of Envisat validation campaigns and obtained measurements with good spatial and temporal coincidence with the satellite (Oelhaf et al., 2003).

The retrieval of atmospheric target parameters from MIPAS-B uses a least squares fitting algorithm based on the forward model KOPRA (Karlsruhe Optimized and Precise Radiative transfer Algorithm) together with a Tikhonov-Phillips regularisation procedure (Stiller, 2000). The resulting vertical resolution lies typically between 2 and 3 km and is therefore comparable to the vertical resolution of the satellite instrument but MIPAS-B has the advantage that many spectra can be averaged for a single retrieval.

Ozone isotopomer enrichment profiles have been derived from both flights (Huck et al., 2004) and it was found that $\delta(^{18}O)$ of asymmetric and $\delta(^{18}O)$ of symmetric ozone, respectively, are larger in mid-latitudes than in Arctic polar regions, as expected due to lower temperatures in the polar winter.

Figure 4 shows the comparison between MIPAS-B and MIPAS vertical mixing ratio profiles of the ozone isotopomers $^{50}O_3$ and their enrichments for the two MIPAS-B validation campaign flights. Mid-latitude profiles and enrichments are in good agreement

ACPD
9, 25127–25158, 2009

for both the asymmetric and the symmetric isotope variants where the sequential estimator gives a more precise representation of the atmospheric state. In polar winter case MIPAS shows much larger profiles and enrichments than MIPAS-B when using the sequential estimator in the retrieval, while comparable enrichments are obtained when using the standard single retrieval. This discrepancy is presumably related to the zonally asymmetric state of the atmosphere in polar winter, and caution should be applied when intepreting the sequential estimator results under such conditions.

5 MIPAS heavy ozone enrichments

5.1 Zonal mean distributions

Figure 5 shows the retrieved zonal mean enrichments for 20 March 2004. The enrichments for the asymmetric isotopomer are apparently noisier than the symmetric isotopomer and this is expected from the error analysis shown in Fig. 2, which suggest a total error for the symmetric isotopomer 2–3 times larger between 20–50 km. MIPAS measurements also indicate that asymmetric heavy ozone is significantly more enriched than the symmetric isotopomer and that the magnitude of these enrichments is ~10% in stratosphere, in agreement with previous observations. Latitudinal and vertical variations appear in both the asymmetric and symmetric $^{50}O_3$ enrichments. The total $^{50}O_3$ enrichment also varies as a function of latitude and altitude. This contradicts ATMOS observations (Irion et al., 1996) and FIRS-2 measurements (Johnson et al., 2000) where no latitudinal and vertical gradient were found, but this may be attributable to the limited latitude and altitude coverage of these observations compared to MIPAS.

ACPD
9, 25127–25158, 2009

5.2 Time series of asymmetric $^{50}O_3$

To investigate the seasonal cycle in the O_3 isotopomer distribution, one or two days per month of full resolution MIPAS data (July 2002–March 2004) have been processed using the sequential estimator described in the sec. 2.3. The choice of dates was a compromise between the number of orbits of Level 1B (i.e. radiometrically and spectrally calibrated geolocated spectra) data available and evenly spaced days in time with the preference of days close to equinoxes and solstices. In full operation there were 72 limb scans per orbit which, with 14 orbits per day, resulted in approximately 1000 profiles per day.

Figure 6 shows an example of the enrichment time series for the ozone isotopomer $^{16}O^{16}O^{18}O$ at 33 km divided into six latitude bands.

For mid-latitudes and equatorial regions the enrichment remains quite stable at around 10% but there is more variability at high latitudes. The south polar region shows a clear annual cycle varying from 0–20%, increasing rapidly during the polar winter, and then decreasing steadily throughout the rest of the year. The arctic region is much noisier but there may be a similar underlying pattern shifted by 6 months.

5.3 Variability with temperature, ozone and methane

Although ATMOS observations (Irion et al., 1996) and FIRS-2 measurements (Johnson et al., 2000) did not find a vertical gradient, Mauersberger et al. (2001) attempted to explain the altitude variation of their stratospheric ozone isotope enrichments, obtained with borne-balloon sampling experiments by temperature variation. Laboratory measurements (Morton et al., 1990) suggested an averaged variation of enrichments with temperature of 0.06% K^{-1}, but this is too small to explain the observed enrichments with altitude by Mauersberger et al. (2001) based on the stratospheric temperature profile. Therefore temperature gradient may not alone account for the observed enrichment variantions.

Figure 7 shows the time series of normalised variations of $^{16}O^{16}O^{18}O$, temperature, methane and standard ozone at 33 km, all retrieved from the same MIPAS spectra. Variations in heavy ozone appear to be positively correlated with the other three parameters in all latitude bands except in equatorial regions where there appears to be an anticorrelation with temperature. Examination of similar plots for 10° latitude bins does not reveal any further details, neither is there any apparent correlation between enrichment and net daylight.

The heavy ozone enrichment appears well-correlated with methane suggesting it acts like a passive tracer. The positive correlation with standard ozone is investigated for nine different altitudes, ranging from 21 km to 47 km, and the results are presented in Fig. 8. The standard ozone abundances have been retrieved using a standard single retrieval approach and the ESA operational microwindows. For altitudes between 27–33 km the asymmetric $^{50}O_3$ enrichments are fairly constant with standard ozone VMR variations, except for Southern polar regions where enrichments increase with increasing ozone and for Norther polar regions where the enrichments appear noiser.

6 Correlations between δ^{18}O and δ^{17}O

MIPAS measurements contain also information on the asymmetric and symmetric $^{49}O_3$ isotopomers although the signal-to-noise is lower due to much lower abundance of ^{17}O relative to oxygen atoms ^{16}O (1:2700). Here the same sequential estimator described above has been used to retrieve $^{17}O^{16}O^{16}O$ and $^{16}O^{17}O^{16}O$ isotopomers jointly with the main and $^{50}O_3$ isotopomers using the microwindows listed in Table 1. The error analysis on the δ values (not shown here) indicates a total error on the asymmetric $^{49}O_3$ below 3% for 24–47 km and on the symmetric $^{49}O_3$ below 5% for 27–42 km. In both cases the total error is dominated by the systematic error component as in the case of $^{50}O_3$ isotopomers.

Figure 9 compares the variability of $^{50}O_3$ and $^{49}O_3$ as a function of nine different MIPAS tangent altitudes. The spread in the measurements of $\delta^{17}O$ is significantly greater than the spread in $\delta^{18}O$. This contradicts the first experimental evidence (Thiemens and Heidenreich, 1983) that the enrichments in ^{17}O and ^{18}O are related to each other with a slope of 1 rather than the typical ∼0.5 dependence. Subsequent measurements demonstrated that the three body reaction between O and O_2 (Reaction R1) results in large enrichments for the heavier isotopomers (Morton et al., 1990), in contraddction with MIPAS results where $\delta^{17}O$ appears to be much larger than $\delta^{18}O$.

7 Conclusions

The Michelson Interferometer for Passive Atmospheric Sounding (MIPAS) observations have been used to retrieve vertical enrichment profiles of stratospheric heavy ozone.

MIPAS enrichments in stratosphere are consistent with those obtained by previous stratospheric observations and lab measurements. The asymmetric heavy ozone is significantly more enriched than the symmetric isotopomer. Both asymmetric and symmetric isotopomer enrichments show latitudinal and vertical variations. Variations in heavy ozone appear to be positively correlated with temperature, methane and standard ozone in all latitude bands except in equatorial regions where there appears to be an anticorrelation with temperature.

The asymmetric and symmetric $^{49}O_3$ isotopomers have also been retrieved from MIPAS measurements. The enrichments of $^{49}O_3$ are much larger than the enrichments of $^{50}O_3$, in contradictions with previous results which predict larger enrichments for heavier isotopomers.

ACPD
9, 25127–25158, 2009

Acknowledgements. We want to thank David Johnson for providing FIRS-2 measurements of the O_3 isotopomers enrichments, Petra Huck and Herman Oelhaf for MIPAS-B measurements of O_3 isotopomers and their enrichments. The authors would like to thank the European Space Agency (ESA) for providing MIPAS L1B data. This work is supported by DARC (Data Assimilation Research Centre), UK.

References

Abbas, M. M., Guo, J., Carli, B., et al.: Heavy ozone distribution in the stratosphere from far-infrared observations, J. Geophys. Res., 92, 13231–13239, 1987. 25131

Anderson, S. M., Morton, J., and Mauersberger, K.: Laboratory measurements of ozone isotopomers by tunable diode laser absorption spectroscopy, Chem. Phys. Lett., 156, 175–180, 1989.

Anderson, S. M., Hulsebusch, D., and Mauersberger, K.: Surprising rate coefficients for four isotopic variants of O + O_2 + M, J. Chem. Phys., 107, 5385–5392, 1997. 25132

Bhattacharya, S. K., Chakraborty, S., Savarino, J., et al.: Low-pressure dependency of the isotopic enrichment in ozone: Stratospheric implications, J. Geophys. Res., 107, 4675, doi:10.1029/2002JD002508, 2002. 25131

Carli, B. and Park, J. H.: Simultaneous measurement of minor stratospheric constituents with emission far-infrared spectroscopy, J. Geophys. Res., 93, 3851–3865, 1988. 25131

ESA, SP-1229: ESA ENVISAT-MIPAS: an instrument for atmospheric chemistry and climate research, European Space Agency, ESTEC, Noordwijck, The Netherlands, 2000. 25133

Dudhia, A., Morris, P. E., and Wells, R. J.: Fast monochromatic radiative transfer calculations for limb sounding, J. Quant. Spectrosc. Ra., 74, 745–756, 2002a. 25134

Dudhia, A., Jay, V., and Rodgers, C. D.: Microwindow selection for high-resolution sounders, Appl. Opt., 41, 3665–3673, 2002b. 25133, 25136

Flaud, J.-M., Piccolo, C., Carli, B., et al.: Molecular line parameters for the MIPAS (Michelson Interferometer for Passive Atmospheric Sounding) experiment, Atmos. Oceanic Opt., 16, 172–182, 2003. 25134

Friedl-Vallon, F., Maucher, G., Seefeldner, M., et al.: Design and characterisation of the balloon-borne Michelson 15 Interferometer for Passive Atmospheric Sounding (MIPAS-B2), Appl. Opt., 43, 3335–3355, 2004. 25140

Huck, P., Oelhaf, H., Wetzel, G., et al.: Determination of vertical profiles of ozone isotopomers and their enrichments in the Arctic polar vortex and in mid-latitudes, Proceeding of the XX Quadrennal Ozone Symposium, Kos, Greece, 1–8 June 2004, 2004. 25140

Irion, F. W., Gunson, M. R., Rinsland, C. P., et al.: Heavy ozone enrichments from ATMOS infrared solar spectra, Geophys. Res. Lett., 23, 2377–2380, 1996. 25131, 25141, 25142

Janssen, C., Günther, J., Mauersberger, K., et al.: Kinetic origin of the ozone isotope effect: a critical analysis of enrichments and rate coefficients, Phys. Chem. Chem. Phys., 3, 4718–4721, 2001. 25130

Janssen, C., Guenther, J., Krankowsky, D., et al.: Temperature dependence of ozone rate coefficients and isotopologue fractionation in ^{16}O–^{18}O oxygen mixture, Chem. Phys. Lett., 367, 34–38, 2003. 25130, 25132

Johnson, D. G., Jucks, K. W., Traub, W. A., et al.: Smithsonian stratospheric far-infrared spectrometer and data reduction system, J. Geophys. Res., 100, 3091–3106, 1995. 25139

Johnson, D. G., Jucks, K. W., Traub, W. A., et al.: Isotopic composition of stratospheric ozone, J. Geophys. Res., 105, 9025–9031, 2000. 25131, 25140, 25141, 25142

Johnston, J. C. and Thiemens, M. H.: Mass independent oxygen isotopic composition of tropospheric ozone from 3 different enviroments, J. Geophys. Res., 102, 25395–25398, 1997. 25131

Kaye, J. A. and Strobel, D. F.: Enhancement of heavy ozone in the Earth's atmosphere, J. Geophys. Res., 88, 8447–8452, 1983. 25130, 25131

Krankowsky, D., Lämmerzahl, P., and Mauersberger, K.: Isotopic measurements of stratospheric ozone, Geophys. Res. Lett., 27, 2593–2595, 2000. 25131, 25132

Lämmerzahl, P., Röckmann, T., Brenninkmeijer, C. A., et al.: Oxygen isotope composition of stratospheric carbon dioxide, Geophys. Res. Lett., 29, 1582, doi:10.1029/2001GL0114343, 2002. 25130, 25131, 25132

Liang, M.-C., Irion, F. W., Weibel, J. D., et al.: Isotopic composition of stratospheric ozone, J. Geophys. Res., 111, 2302, doi:10.1029/2005JD006342, 2006. 25131

Mauersberger, K.: Measurement of heavy ozone in the stratosphere, Geophys. Res. Lett., 8, 935–939, 1981. 25129, 25131

Mauersberger, K., Erbacher, B., Krankowsky, D., et al.: Ozone isotope enrichment: Isotopomer-specific rate coefficients, Science, 283, 370–372, 1999. 25132

Mauersberger, K., Lämmerzahl, P., and Krankowsky, D.: Stratospheric ozone isotope enrichments-revised, Geophys. Res. Lett., 16, 3155–3158, 2001. 25130, 25131, 25132, 25142

Meier, A. and Notholt, J.: Determination of isotopic abundances of heavy O3 as observed in Arctic ground-based FTIR-spectra, Geophys. Res. Lett., 23, 551–554, 1996. 25131

Morton, J., Barnes, J., Schueler, B., et al.: Laboratory studies of heavy ozone, J. Geophys. Res., 95, 901–907, 1990. 25132, 25142, 25144

Oelhaf, H., Friedl-Vallon, F., Kleinert, A., et al.:, ENVISAT validation with MIPAS-B, in: Proc. ENVISAT Validation 5 Workshop, 9–13 December, 2002, ESRIN, Frascati, Italy, CD-ROM, vol. SP-531, ESA Publications Division, ESTEC, Postbus 299, 2200AG Noordwijk, The Netherlands, 2003. 25140

Ridolfi, M., Carli, B., Carlotti, M., et al.: Optimised forward model and retrieval scheme for MIPAS near-real-time data processing, Appl. Opt., 39(8), 1323–1340, 2000. 25133

Raspollini, P., Belotti, C., Burgess, A., Carli, B., Carlotti, M., Ceccherini, S., Dinelli, B. M., Dudhia, A., Flaud, J.-M., Funke, B., Höpfner, M., Lòpez-Puertas, M., Payne, V., Piccolo, C., Remedios, J. J., Ridolfi, M., and Spang, R.: MIPAS level 2 operational analysis, Atmos. Chem. Phys., 6, 5605–5630, 2006, http://www.atmos-chem-phys.net/6/5605/2006/.

Rodgers, C. D.: Inversion Methods for atmospheric sounding: theory and practice, World Scientific Publishing, 2000. 25134, 25135

Payne, V. H., Noone, D., Dudhia, A., et al.: Global satellite measurements of HDO and implications for understanding the entry of water vapour into the stratosphere, Q. J. Roy. Meteor. Soc., 133(627), 1459–1471, 2007. 25133, 25138

Schueler, B., Morton, J., and Mauersberger, K.: Measurements of isotopic abundances in collected stratospheric ozone samples, Geophys. Res. Lett., 17, 1295–1298, 1990. 25131

Steinwagner, J., Milz, M., von Clarmann, T., Glatthor, N., Grabowski, U., Höpfner, M., Stiller, G. P., and Röckmann, T.: HDO measurements with MIPAS, Atmos. Chem. Phys., 7, 2601–2615, 2007, http://www.atmos-chem-phys.net/7/2601/2007/. 25133, 25138

Stiller, G. P.: The Karlsruhe Optimized and Precise Radiative transfer Algorithm (KOPRA), Forschungszentrum Karlsruhe, Wissenschaftliche Berichte, Bericht Nr. 6487, 2000. 25140

Thiemens, M. H. and Heidenreich, J. E.: The mass indipendent fractionation of oxygen – A novel isotope effect and its possible cosmochemical implications, Science, 219, 1073–1075, 1983. 25129, 25131, 25132, 25144

Yung, Y. L., DeMore, W. B., and Pinto, J. P.: Isotopic exchange between carbon dioxide and ozone via O(^{1}D) in the stratosphere, Geophys. Res. Lett., 18, 13–16, 1991. 25129

Yung, Y. L., Lee, A. Y. T, Irion, F. W., et al.: Carbon dioxide in the atmosphere: Isotopic exchange with ozone and its use as a tracer in the middle atmosphere, J. Geophys. Res., 102, D9, 10857–10866, 1997. 25129

Table 1. Spectral and altitude ranges of the microwindows selected for the ozone isotope retrievals.

No	Spectral range [cm^{-1}]	Altitude range [km]
1	1020.650–1023.650	6.0–68.0
2	1088.000–1091.000	6.0–68.0
3	1043.225–1044.675	6.0–39.0
4	969.200–969.625	12.0–36.0
5	1042.125–1042.875	47.0–68.0
6	960.950–963.950	18.0–36.0
7	1053.975–1055.350	15.0–68.0
8	1037.825–1038.375	52.0–68.0
9	713.800–714.500	18.0–30.0

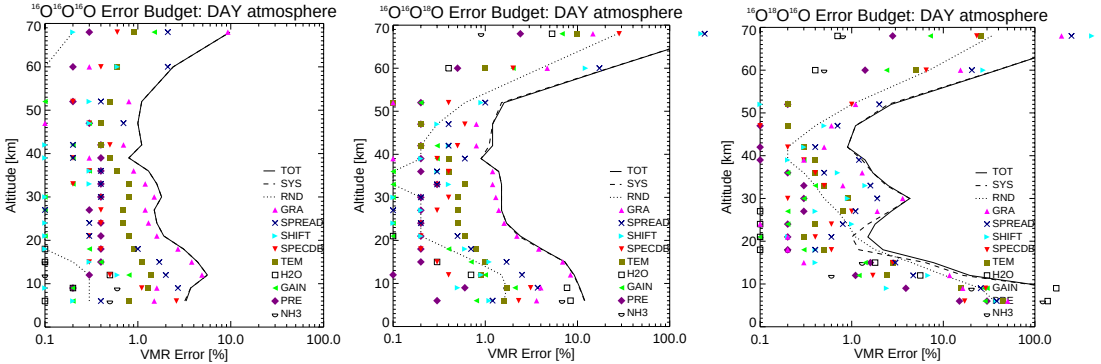

Fig. 1. Estimated error contributions provided by the microwindow selection for main (left) $^{48}O_3$ isotopomer and the asymmetric (central) and symmetric (right) $^{50}O_3$ isotopomers, when applying the sequential estimator approach. The total error (solid line "TOT") is dominated by the total systematic error (dashed line "SYS"). Symbols show individual systematic errors: the most significant error is given by assuming horizontally homogeneous atmospheres "GRA", followed by calibration errors (instrument line shape calibration "SPREAD", spectral calibration "SHIFT"), uncertainties in the spectroscopic line parameters "SPECDB".

ACPD
9, 25127–25158, 2009

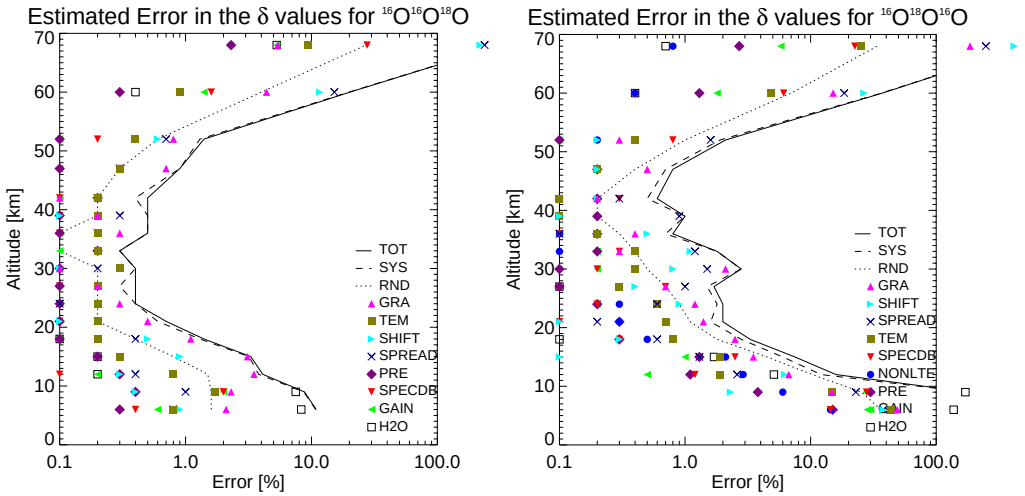

Fig. 2. Estimated error contributions for the δ values for asymmetric (left) and symmetric (right) $^{50}O_3$ isotopomers, when applying the sequential estimator retrieval on about 50 profiles per 10° latitude band/day. As in Fig. 1, each symbol represents different systematic components which affect the retrieval, solid line the total error, dotted line the random error and dashed line the total systematic error.

ACPD
9, 25127–25158, 2009

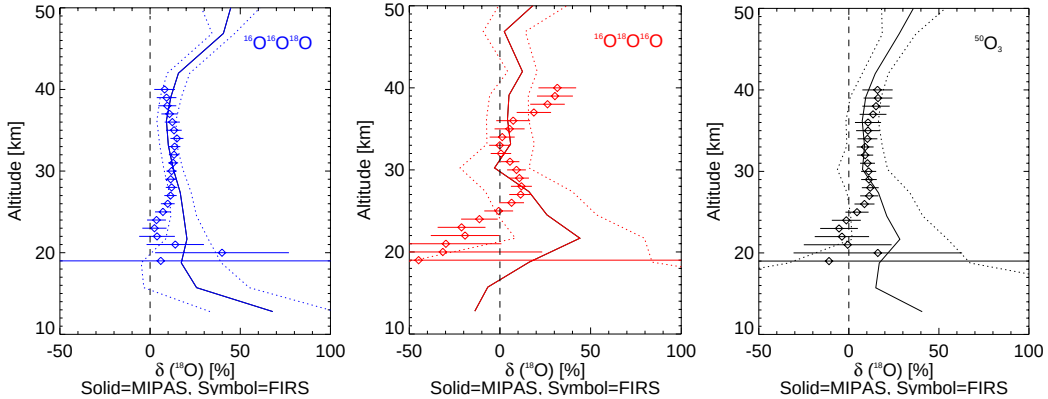

Fig. 3. Comparison of midlatitude averaged enhancements between MIPAS (solid lines) and FIRS-2 (symbols) for asymmetric (top), symmetric (middle) and total (right) $\delta(^{18}O)$, respectively. Error bars for FIRS-2 and dotted curves for MIPAS indicate the estimated precision.

ACPD
9, 25127–25158, 2009

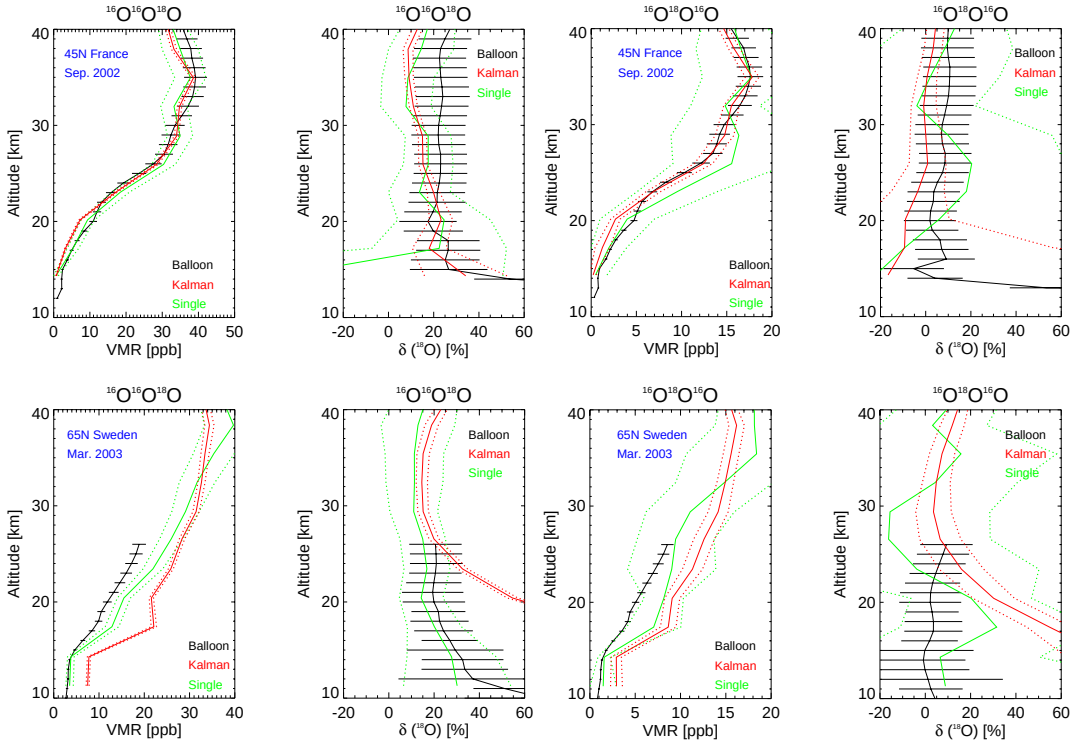

Fig. 4. Comparison between MIPAS-B (black) and MIPAS (red when using the sequential estimator and green when using the standard single retrieval) for the two MIPAS-B flights, 43.7° N in September 2002 (top panels) and 67.5° N in March 2003 (bottom panels): vertical mixing ratio profiles (left) and enrichments (right) of asymmetric and symmetric $^{50}O_3$. Only random errors are plotted: in the case of MIPAS (red) the random error on the final profile is greatly reduced by the sequential estimator (approximately to a seventh of an individual retrieval error).

ACPD
9, 25127–25158, 2009

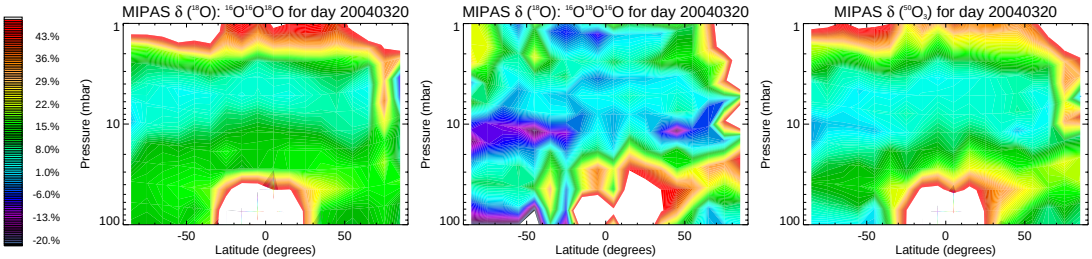

Fig. 5. Zonal mean distribution of enrichments for asymmetric (left), symmetric (middle) and net (right) $^{50}O_3$, respectively.

ACPD
9, 25127–25158, 2009

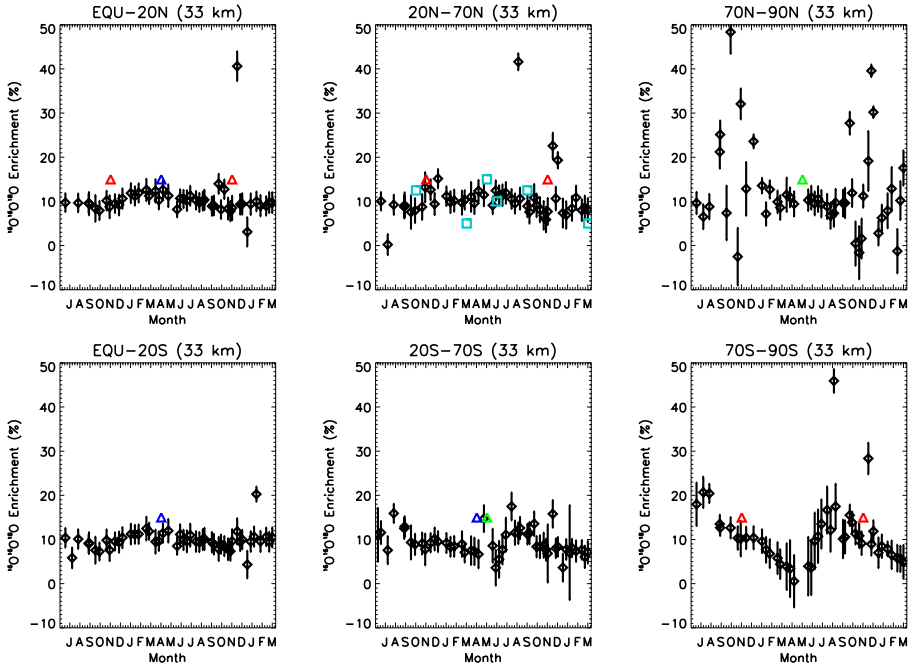

Fig. 6. Time series from July 2002 to March 2004 of δ^{18}O for the ozone isotopomer $^{16}O^{16}O^{18}O$ at altitude 33 km for six latitude bands as a function of time. Error bars indicate estimated precision on the mean enrichment value at 33 km. Other symbols represent previous observations at similar locations: light blue squares (20–70° N panel) show FIRS-2 values from the six balloon flights which took place between 1989 and 1994; triangles are the ATMOS values from ATLAS-3 (November 1994) in red, ATLAS-2 (May 1993) in green and ATLAS-1 (April 1992) in blue.

ACPD
9, 25127–25158, 2009

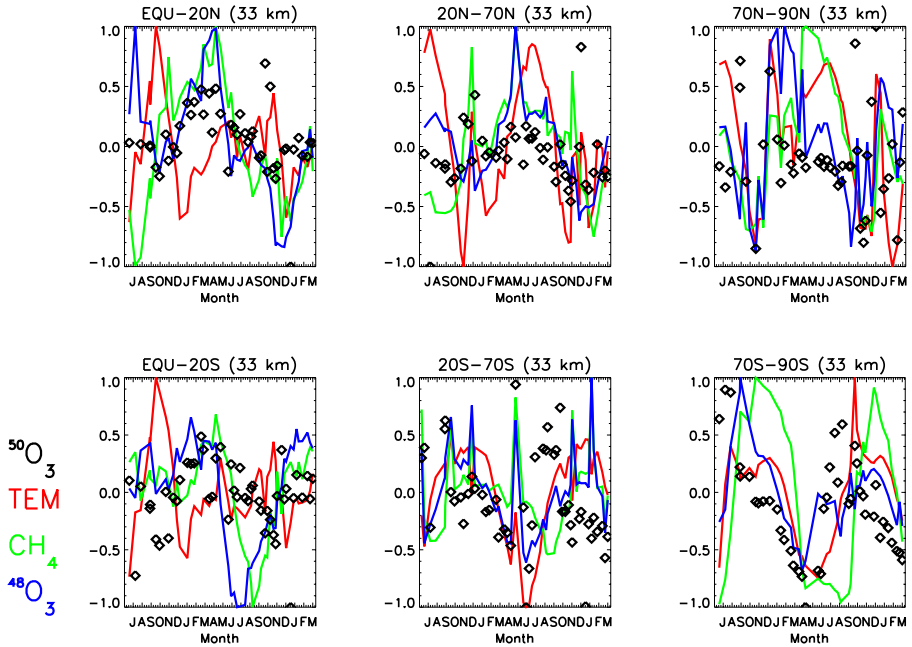

Fig. 7. Time series of normalised variations of $^{50}O_3$ enrichment (black symbols), temperature (red line), methane (green line) and standard ozone (blue line) at 33 km for the same six latitude bands of Fig. 6.

ACPD
9, 25127–25158, 2009

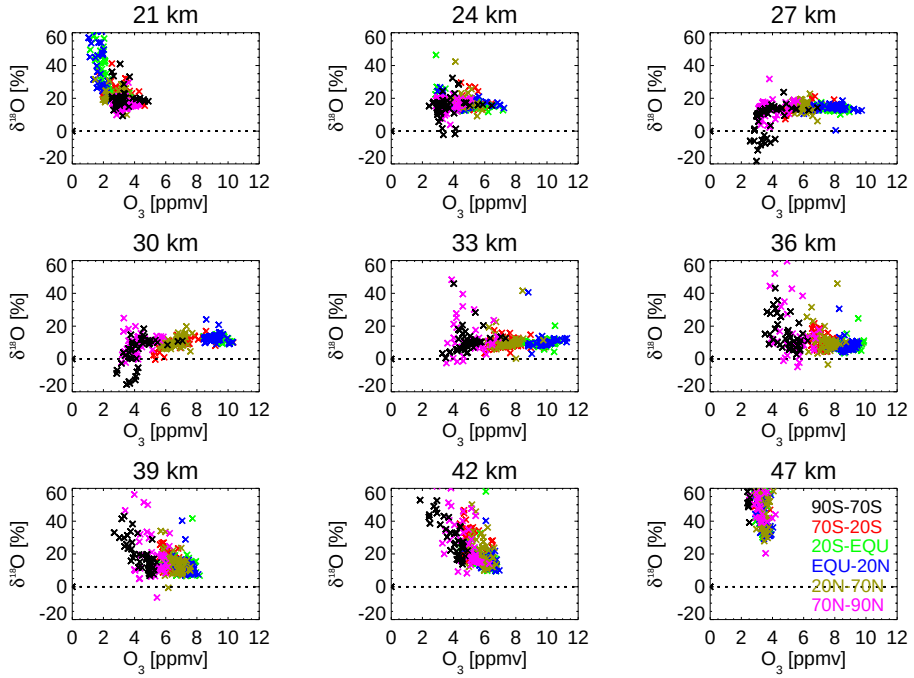

Fig. 8. Correlation between enrichment of $^{16}O^{16}O^{18}O$ and $^{48}O_3$ abundance for 6 latitude bands and nine MIPAS tangent altitudes (from 21 to 47 km).

ACPD
9, 25127–25158, 2009

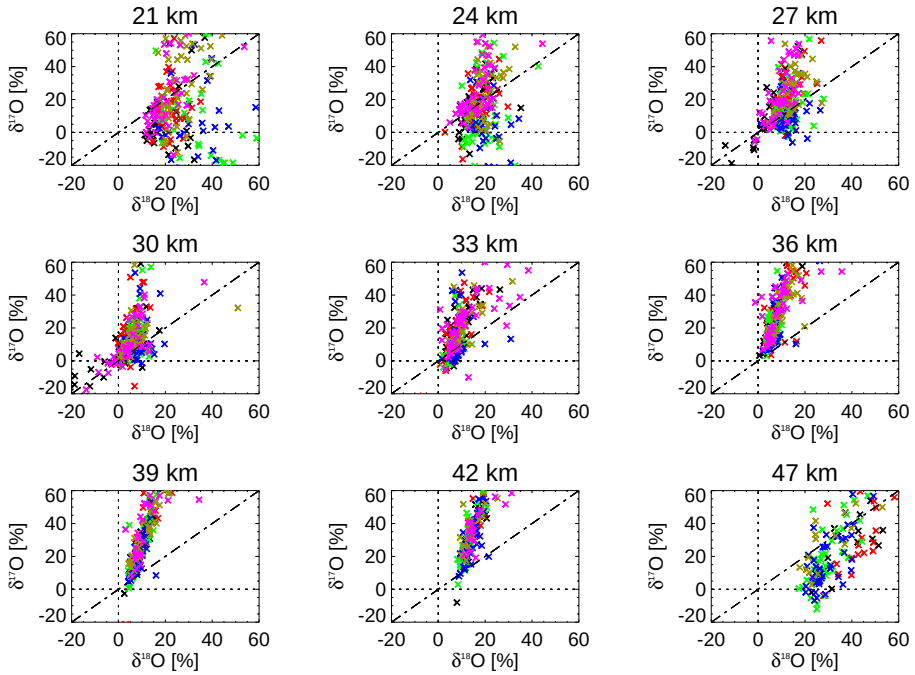

Fig. 9. Variability of MIPAS measurements of $^{50}O_3$ and $^{49}O_3$ for nine different MIPAS tangent altitudes. Different colors correspond to different latitude bands (same color code as Fig. 8).

ACPD
9, 25127–25158, 2009